

# Sub-Riemannian Fast Marching in $SE(2)$

Gonzalo Sanguinetti<sup>1</sup> (✉), Erik Bekkers<sup>2</sup>, Remco Duits<sup>1,2</sup>,  
Michiel H.J. Janssen<sup>1</sup>, Alexey Mashtakov<sup>2</sup>, and Jean-Marie Mirebeau<sup>3</sup>

<sup>1</sup> Department of Mathematics and Computer Science,  
Eindhoven University of Technology, Eindhoven, The Netherlands  
{G.R.Sanguinetti,R.Duits,M.H.J.Janssen}@tue.nl

<sup>2</sup> Department of Biomedical Engineering,  
Eindhoven University of Technology, Eindhoven, The Netherlands  
{E.J.Bekkers,A.Mashtakov}@tue.nl

<sup>3</sup> Laboratory Ceremade, CNRS, University Paris-Dauphine, Paris, France  
mirebeau@ceremade.dauphine.fr

**Abstract.** We propose a Fast Marching based implementation for computing sub-Riemannian (SR) geodesics in the roto-translation group  $SE(2)$ , with a metric depending on a cost induced by the image data. The key ingredient is a Riemannian approximation of the SR-metric. Then, a state of the art Fast Marching solver that is able to deal with extreme anisotropies is used to compute a SR-distance map as the solution of a corresponding eikonal equation. Subsequent backtracking on the distance map gives the geodesics. To validate the method, we consider the uniform cost case in which exact formulas for SR-geodesics are known and we show remarkable accuracy of the numerically computed SR-spheres. We also show a dramatic decrease in computational time with respect to a previous PDE-based iterative approach. Regarding image analysis applications, we show the potential of considering these data adaptive geodesics for a fully automated retinal vessel tree segmentation.

**Keywords:** Roto-translation group · Sub-riemannian · Fast marching

## 1 Introduction

In this article we study a curve optimization problem in the space of coupled positions and orientations  $\mathbb{R}^2 \times S^1$ , which we identify with roto-translation group  $SE(2)$ . We aim to compute the shortest curve  $\gamma(t) = (x(t), y(t), \theta(t)) \in SE(2)$  that connects 2 points  $\gamma(0) = (x_0, y_0, \theta_0)$  and  $\gamma(L) = (x_1, y_1, \theta_1)$  with the restriction that the curve is "lifted" from a planar curve in the sense that the third variable  $\theta$  is given by  $\theta(t) = \arg(\dot{x}(t) + i\dot{y}(t))$ , see Fig. 1. This restriction imposes a so-called sub-Riemannian (through the text we denote sub-Riemannian as SR)

---

G. Sanguinetti—The research leading to the results of this article has received funding from the European Research Council under the (FP7/2007-2014-)ERC grant ag. no. 335555 and from (FP7-PEOPLE-2013-ITN)EU Marie-Curie ag. no. 607643.

metric that constrains the tangent vectors to the curve to be contained in a subspace of the tangent space at every point. This subspace is a plane, which differs from point to point, and is the set of all possible tangents to curves in  $SE(2)$  that are lifted from smooth planar curves. A SR-metric is a degenerated Riemannian metric in which one direction, the one perpendicular to the path in this case, is prohibited (i.e. it has infinite cost). On top of the SR-metric, we also consider a smooth external cost, which weights the metric tensor in every location and allows for data-adaptivity.

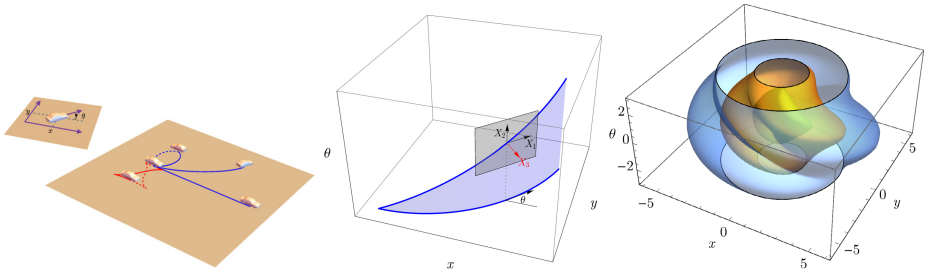


**Fig. 1.** **Left:** the sub-Riemannian problem in  $SE(2)$  can be identified with that of a car with two controls (giving gas and steering the wheel). **Center:** the paths are “lifted” into curves in  $SE(2) = \mathbb{R}^2 \times S^1$  with tangent vectors constrained to the plane spanned by the vector fields  $X_1$  and  $X_2$  (eq. (1)) associated with the controls. **Right:** the SR-spheres (for  $t = 2, 4$  and  $6$ ) obtained via the FM-LBR method.

Essentially, the SR-problem in  $SE(2)$  is that of a car that can go forward, backward and rotate (a so-called Reeds-Shepp car) so the possible states of the car form a 3D manifold given by the position  $(x, y)$  and the orientation  $\theta$  of the car. Then, admissible trajectories of the car are parametrized by only 2 control variables associated to the car moving along a straight line (giving gas) and to a change of direction (turning the steering wheel). The fact that the car cannot step aside infinitesimally imposes the SR-geometry. Finally, the curve optimization problem is to find among all possible trajectories between two given states, the one with minimal SR-length.

In image analysis the SR-geodesics in  $SE(2)$  have been proposed in [4] as candidates for completion of occluded contours. Here, the geometrical structure is used as a model for the functional architecture of the primary visual cortex. This model has proven to be valuable in numerous applications [3–6], and it becomes powerful when combined with the orientation score theory [6] that allows for an invertible stable transformation between 2D images and functions on the  $SE(2)$  group. The main advantage of considering this space of positions and orientations is that intersecting curves are automatically disentangled, and therefore the processing in the extended domain naturally deals with complex structures such as crossing.

Sub-Riemannian geodesics in the uniform cost case (the same cost for all the  $SE(2)$  elements) were studied by several authors (e.g. [5, 12]). Recently, a

wavefront propagation method for computing SR-geodesics that also deals with the non-uniform cost case has been proposed in [1]. This method is an extension to the SR-case of a classical PDE-approach for computing cost-adaptive geodesics used in computer vision, where the metric tensor is induced by the image itself. The main idea is to consider propagation of equidistant surfaces described by level sets of the viscosity solution of an eikonal equation, while subsequent backtracking gives the geodesics. In order to solve the eikonal equation, the authors rely on a computationally expensive iterative approach based on a left-invariant finite-difference discretization of the PDE combined with a suitable upwind scheme.

Here, again in the spirit of computer vision methods, we aim to compute the SR-distance map using a Fast Marching method [13]. This technique, closely related to Dijkstra's method for computing the shortest paths on networks, allows for a significant speed up in the computation of the eikonal equation's viscosity solution. The main difficulty in our case is that classical solvers are unable to deal with the extreme (degenerated) anisotropy of the SR-metric. Recently, a modification of the Fast Marching method using lattice basis reduction (FM-LBR) that solves this problem was introduced in [9] (code available at <https://github.com/Mirebeau/ITKFM>). Then, the purpose of this paper is to show how the SR-curve optimization problem can be numerically solved using the FM-LBR method. The key aspects to consider are a Riemannian relaxation of the SR-problem and expressing the resulting metric tensor as a matrix-induced Riemannian metric in a fixed Cartesian frame. We develop these ideas in the Theory section. Then, two experiments are presented. The first one considers the uniform cost case ( $\mathcal{C} = 1$ ) and shows that the FM-LBR based method presented here outperforms the iterative implementation in [1] in terms of CPU time, while keeping a similar accuracy. The advantages of considering data-adaptive SR-geodesics for extracting blood vessels in retinal images are illustrated in the second experiment.

## 2 Theory

**Problem Formulation.** Let  $g = (x, y, \theta)$  be an element of  $SE(2) = \mathbb{R}^2 \times S^1$ . A natural moving frame of reference in  $SE(2)$  is described by the left-invariant vector fields  $\{X_1, X_2, X_3\}$  spanning the tangent space at each element  $g$ :

$$X_1 = \cos \theta \partial_x + \sin \theta \partial_y, \quad X_2 = \partial_\theta, \quad X_3 = -\sin \theta \partial_x + \cos \theta \partial_y. \quad (1)$$

The tangents  $\dot{\gamma}(t)$  along curves  $\gamma(t) = (x(t), y(t), \theta(t)) \in SE(2)$  can be written as  $\dot{\gamma}(t) = \sum_{i=1}^3 u^i(t) X_i|_{\gamma(t)}$ . Only the curves with  $u^3 = 0$  are liftings of planar curves (see fig. 1). Then, the tangents to curves that are liftings of planar curves are expressed as  $\dot{\gamma}(t) = u^1(t) X_1|_{\gamma(t)} + u^2(t) X_2|_{\gamma(t)}$  and they span the so-called distribution  $\Delta = \text{span}\{X_1, X_2\}$ . Now, the triplet  $(SE(2), \Delta, G_0)$  defines a sub-Riemannian manifold with inner product  $G_0$  given by:

$$G_0(\dot{\gamma}, \dot{\gamma}) = \mathcal{C}(\gamma)^2 \left( \beta^2 |\dot{x} \cos \theta + \dot{y} \sin \theta|^2 + |\dot{\theta}|^2 \right). \quad (2)$$

In view of the car example (see Fig. 1), the parameter  $\beta > 0$  balances between the cost of giving gas (the  $X_1$  direction) and the turning of the wheel (the  $X_2$  direction). A smooth function  $\mathcal{C} : SE(2) \rightarrow [\delta, 1]$ ,  $\delta > 0$  is the given external cost. In order to keep the notation sober during this paper, we do not indicate the dependence of  $G_0$  on the cost  $\mathcal{C}$  nor that it also depends on the curve  $\gamma$ . Note that the subindex 0 in the metric tensor recalls the SR-structure imposed by allowing null displacement in the  $X_3$  direction (i.e. infinite cost for the car to move aside). This choice of notation will become clear later in the text. Now, optimal paths  $\gamma$  of the car in our extended position orientation space are solutions of the problem:

$$W(g) = d_0(g, e) = \min \left\{ \int_0^T \|\dot{\gamma}(t)\|_0 dt \mid \dot{\gamma} \in \Delta, \gamma(0) = e, \gamma(T) = g, T \geq 0 \right\} \quad (3)$$

where  $e = (0, 0, 0)$  is the origin, where  $\|\dot{\gamma}(t)\|_0 = \sqrt{G_0(\dot{\gamma}(t), \dot{\gamma}(t))}$  is the SR-norm and  $d_0$  is the SR-distance on  $SE(2)$ .

**Riemannian Approximation.** It is possible to obtain a Riemannian approximation of the SR-problem by expanding the metric tensor in eq. (2) to:

$$G_\epsilon(\dot{\gamma}, \dot{\gamma}) = G_0(\dot{\gamma}, \dot{\gamma}) + \epsilon^{-2} \mathcal{C}(\gamma)^2 \beta^2 |\dot{x} \sin \theta - \dot{y} \cos \theta|^2, \quad (4)$$

where  $\epsilon$  determines the amount of anisotropy between  $X_3$  and  $\Delta$ . This definition bridges the SR-case, obtained at the limit  $\epsilon \downarrow 0$ , with the full Riemannian metric tensor when  $\epsilon = 1$  (isotropic in the spatial directions  $X_1$  and  $X_3$ ). Actually, it is easy to verify that if  $\mathcal{C} = 1$  and  $\beta = \epsilon = 1$ , then  $G_1(\dot{\gamma}, \dot{\gamma}) = |\dot{x}|^2 + |\dot{y}|^2 + |\dot{\theta}|^2$ . Also, by replacing  $G_0$  with  $G_\epsilon$  in eq. (3) we can construct a Riemannian norm  $\|\cdot\|_\epsilon$  and a distance  $d_\epsilon$  satisfying  $\lim_{\epsilon \downarrow 0} \|\cdot\|_\epsilon = \|\cdot\|_0$  and  $\lim_{\epsilon \downarrow 0} d_\epsilon = d_0$ .

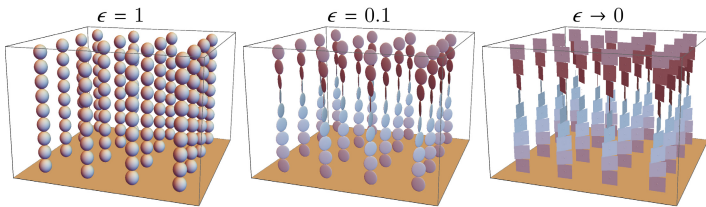


**Fig. 2.** Each ellipsoid represents the Tissot’s indicatrix of the metric  $G_\epsilon$  at different elements  $g \in SE(2)$  (for the case  $\mathcal{C}(g) = 1$  and  $\beta = 1$ ). The parameter  $\epsilon$  in eq. (4) bridges the Riemannian case with the SR-one. When  $\epsilon = 1$  each direction has the same cost. At the limit  $\epsilon \downarrow 0$ , the direction  $X_3$  has infinite cost and the distribution  $\Delta$  appears.

**Solution Via the Eikonal Equation.** Now we can present the eikonal system that solves the problem (3) by computing the distance map  $W(g)$  as proved in [1]. Following [4], let us introduce some differential operators that will simplify the

notation of the remaining equations. Let  $U$  be a smooth function  $U : SE(2) \rightarrow \mathbb{R}$ . The Riemannian gradient  $\nabla^\epsilon$ , computed as the inverse of the metric tensor  $G_\epsilon$  acting on the derivative, is given by:

$$\nabla^\epsilon U := G_\epsilon^{-1}dU = \mathcal{C}^{-2}\beta^{-2}(X_1U)X_1 + \mathcal{C}^{-2}(X_2U)X_2 + \epsilon^2\mathcal{C}^{-2}\beta^{-2}(X_3U)X_3. \quad (5)$$

Then, the norm of the gradient  $\nabla^\epsilon$  is given by:

$$\|\nabla^\epsilon U\|_\epsilon = \sqrt{\mathcal{C}^{-2}\beta^{-2}|X_1U|^2 + \mathcal{C}^{-2}|X_2U|^2 + \epsilon^2\mathcal{C}^{-2}\beta^{-2}|X_3U|^2}. \quad (6)$$

Thus, the eikonal system that characterizes the propagation of equidistant surfaces reads as:

$$\begin{cases} \|\nabla^\epsilon W(g)\|_\epsilon = 1, & \text{if } g \neq e, \\ W(e) = 0. \end{cases} \quad (7)$$

When  $\epsilon \downarrow 0$  this system becomes the SR-eikonal system in [1, eq.3] where it was proved that the unique viscosity solution is indeed the geodesic distance map from the origin  $W(g) = d_\epsilon(g, e)$ . Then, SR-geodesics are the solutions  $\gamma_b(t)$  of the following ODE system for backtracking:

$$\begin{cases} \dot{\gamma}_b(t) = -\nabla^\epsilon(W(\gamma_b(t))), & t \in [0, T] \\ \gamma_b(0) = g. \end{cases} \quad (8)$$

**The Metric Matrix-Representation in the Cartesian Frame.** A symmetric matrix  $M_\epsilon$  representing the anisotropic metric in the frame  $\{\partial_x, \partial_y, \partial_\theta\}$  can be obtained by a basis transformation from the varying frame  $\{X_1, X_2, X_3\}$  (see [4, Sec.2.6]):

$$M_\epsilon = \begin{pmatrix} \cos \theta & 0 & -\sin \theta \\ \sin \theta & 0 & \cos \theta \\ 0 & 1 & 0 \end{pmatrix} \begin{pmatrix} \mathcal{C}^2\beta^2 & 0 & 0 \\ 0 & \mathcal{C}^2 & 0 \\ 0 & 0 & \epsilon^{-2}\mathcal{C}^2\beta^2 \end{pmatrix} \begin{pmatrix} \cos \theta & 0 & -\sin \theta \\ \sin \theta & 0 & \cos \theta \\ 0 & 1 & 0 \end{pmatrix}^T. \quad (9)$$

Here the diagonal matrix in the middle encodes the anisotropy between the  $X_i$  directions while the other 2 rotation matrices are the basis transformation. Note that the columns are the coordinates of the varying frame in the fixed frame, e.g.  $X_1 = \cos \theta \partial_x + \sin \theta \partial_y + 0 \partial_\theta$ . Then, the metric tensor can be written as  $G_\epsilon(\dot{\gamma}, \dot{\gamma}) = \dot{\gamma}(t)M_\epsilon\dot{\gamma}(t)$ , with  $\dot{\gamma}(t) = (\dot{x}(t), \dot{y}(t), \dot{\theta}(t))$ . Using this convention, the eikonal system (7) in the fixed frame can be expressed as:

$$\begin{cases} \nabla^T W(g)M_\epsilon^{-1}\nabla W(g) = 1, & \text{if } g \neq e, \\ W(e) = 0, \end{cases} \quad (10)$$

where  $\nabla = (\partial_x, \partial_y, \partial_\theta)^T$  is the usual Euclidean gradient. The same holds for the backtracking equation (8) which writes:

$$\begin{cases} \dot{\gamma}_b(t) = -M_\epsilon^{-1}\nabla W(\gamma_b(t)), & t \in [0, T] \\ \gamma_b(0) = g. \end{cases} \quad (11)$$

Note that when approaching the SR-case, the  $\lim_{\epsilon \downarrow 0} M_\epsilon$  does not exist but the  $\lim_{\epsilon \downarrow 0} M_\epsilon^{-1}$  is well defined in Eq. (11).

**Anisotropic Fast Marching.** We can now immediately identify Eq. (10) with [9, eq. 0.1] and then solve the eikonal system via the FM-LBR method. Our empirical tests show that  $\epsilon = 0.1$ , which gives an anisotropy ratio  $\kappa = 0.01$  (see [9, eq. 0.5]), is already a good approximation of the SR-case and is the value used in the following experiments.

### 3 Experiments and Applications

**Validation Via Comparison in Uniform Cost Case.** The exact solutions of the SR-geodesic problem for the case  $\mathcal{C} = 1$  are known (see [12] for optimal synthesis of the problem). Therefore, and similar to what is done in [1], we consider this case as our golden standard. Here, we want to compare both the computational time and the accuracy achieved in the calculation of the discrete SR-distance map  $W(g)$ , which is the solution of the eikonal system (7) when  $\epsilon \downarrow 0$ .

Let us set  $\beta = 1$  and consider a grid  $\mathcal{G}_s = \{(x_i, y_j, \theta_k) \in SE(2)\}$  with uniform step size  $s$ , where  $x_i = is$ ,  $y_j = js$ ,  $\theta_k = ks$ , the indices  $i, j, k \in \mathbb{Z}$  such that  $|x_i| \leq 2\pi$ ,  $|y_j| \leq 2\pi$  and  $-\pi + s \leq \theta_k \leq \pi$ . Then we compute the discrete geodesic distance map  $W(g)$  on  $\mathcal{G}_s$  using the iterative method in [1] and the FM-LBR. In order to measure the accuracy of the achieved solutions we follow the method explained in detail in [1]. There, by solving the initial value problem from the origin  $e$ , a set of arc length parametrized SR-geodesics is computed such that SR-spheres of radius  $t$  are densely sampled. Then, the endpoints  $g = (x, y, \theta)$  of each geodesic is stored in a list together with its length  $t$ . Finally, we define the max relative error as  $E_\infty(t) = \max(|W(g) - t|/t)$  where the max is taken over all the endpoints  $g$  and where the value of  $W(g)$  is obtained by bi-linearly interpolating the numerical solutions of eq. (7) computed on the grid  $\mathcal{G}_s$ . The results and comparisons are presented in Fig. 3. Here we solved the eikonal equation in increasingly finer grids  $\mathcal{G}_s$  obtained by setting the step size  $s = \pi/n$ ,  $n \in \mathbb{N}^+$ . Note that the size of  $\mathcal{G}_s$  is then  $(2n+1)(2n+1)(n-1)$ . The graph in Fig. 3(left) shows the comparison of the accuracy achieved in the computation of the SR-sphere of radius  $t = 4$  when  $n$  increases. The behaviour for SR-spheres of different radius is similar. The CPU time is compared in Fig. 3(center). The 3rd plot illustrates the method for computing the accuracy. The orange surface is the SR-sphere of radius  $t = 4$  computed with the FM-LBR method on a grid corresponding to  $n = 101$ . The points are the geodesic endpoints, their color is proportional to the error of the FM-LBR (blue-low, green-medium, red-high error). The first observation is that even though the iterative method is more accurate, both methods seem to have the same order of convergence (the slope in the log-log graphs) when the grid resolution increases. This seems reasonable as both methods use first order approximations of the derivatives. Also, we hypothesise that the offset in favour of the iterative method is due to the Riemannian approximation of the SR-metric (i.e. selecting  $\epsilon = 0.1$ ), but this needs

further investigation. The second key observation is that the CPU time increases dramatically with  $n$  for the iterative method. Therefore, it is clear that we can achieve the same accuracy using the FM-LBR but with much less computational effort, which is of vital importance in the subsequent application.

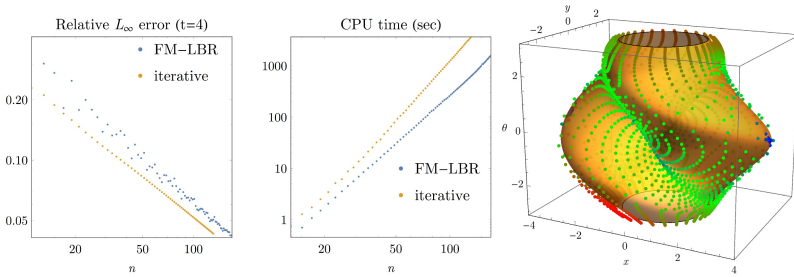


**Fig. 3.** Validation via comparison in the uniform cost case. The experiment (illustrated on the left, see the text) shows that even though the iterative method in [1] is more accurate we can still achieve with the FM-LBR method better results and with less CPU effort, just by increasing the grid sampling.

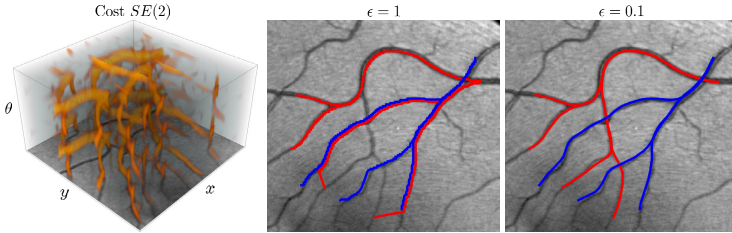


**Fig. 4.** Tracking of blood vessels in retinal images via cost adaptive SR-geodesics (see experiment details in [1]). **Left:** the cost obtained from the image (orange indicates locations with low cost). **Center:** Tracking in the full ( $\epsilon = 1$ ) Riemannian case. **Right:** Tracking with the approximated ( $\epsilon = 0.1$ ) SR-geodesics.

**Application to Retinal Vessel Tree Extraction.** The analysis of the blood vessels in images of the retina provides with early biomarkers of diseases such as diabetes, glaucoma or hypertensive retinopathy [7]. For these studies, it is important to track the structural vessel tree, a difficult task especially because of the crossovers and bifurcations of the vessels. Some existing techniques [1, 10] rely on considering an extended (orientation and/or scale) domain to deal with this issue. Moreover, in [1] promising results were obtained by formulating the vessel extraction as a SR-curve optimization problem with external cost obtained through some wavelet-like transformation of the 2D images. In the previous experiment, we have shown that our proposed FM-LBR based implementation

computes in practice the same geodesics as the iterative method in [1]. Therefore, by simply replacing the eikonal equation solver in [1] we can obtain the same results but with a dramatic decrease of the computational demands (both CPU time and memory). The example in Fig. 4 shows the advantages of considering the SR-metric in performing the vessel tree extraction. In this case (a patch of size  $200 \times 200$  with 64 orientations considered) the iterative method computed the distance map in approximately 1 hour while the FM-LBR did the same in 20 seconds. For the experiments details we refer to [1], for more examples see [www.bmia.bmt.tue.nl/people/RDuits/Bekkersexp.zip](http://www.bmia.bmt.tue.nl/people/RDuits/Bekkersexp.zip).

## 4 Conclusions

Over the last decade, some authors [4–6] have shown the advantages of considering the roto-translation group embedded with a SR-geometry as a powerful, rich tool in some image analysis related problems or for the geometrical modelling of the visual perception. In our opinion, 2 obstacles have prevented this framework to become more popular amongst engineers: the expensive computational demands involved (resulting of considering the extended orientation space) and the lack of efficient numerical methods able to deal with the extreme (degenerated) anisotropy imposed by the SR-metric. These obstacles are addressed by the main contribution of this work, which is solving (up to our knowledge for the first time) the SR-geodesic problem using a Fast Marching based implementation. To be able to achieve this, we rely on the FM-LBR solver recently introduced in [9] and show that even when relaxing the SR-restriction by a Riemannian approximation of the metric we achieve excellent numerical convergence, but much faster than with the approach in [1]. Regarding the retinal imaging application our promising preliminary studies suggest that it is at least feasible to aim for a full vessel tree segmentation as the solution of a single optimization problem, but this requires further investigation. Future work will pursue extension of this method to the 3D-rototranslation group  $SE(3)$  and the applications in neuroimaging and 3D-vessel segmentation.

## References

1. Bekkers, E., Duits, R., Mashtakov, A., Sanguinetti, G.: A PDE approach to Data-Driven Sub-Riemannian Geodesics. SIIMS (In press)
2. Benmansour, F., Cohen, L.D.: Tubular Structure Segmentation Based on Minimal Path Method and Anisotropic Enhancement. IJCV **92**(2), 192–210 (2011)
3. Ben-Yosef, G., Ben-Shahar, O.: A tangent bundle theory for visual curve completion. PAMI **34**(7), 1263–1280 (2012)
4. Citti, G., Sarti, A.: A Cortical Based Model of Perceptual Completion in the Roto-Translation Space. JMIV **24**(3), 307–326 (2006)
5. Duits, R., Boscain, U., Rossi, F., Sachkov, Y.: Association Fields via Cuspless Sub-Riemannian Geodesics in  $SE(2)$ . JMIV **49**(2), 384–417 (2014)
6. Franken, E., Duits, R.: Crossing-Preserving Coherence-Enhancing Diffusion on Invertible Orientation Scores. IJCV **85**(3), 253–278 (2009)



7. Ikram, M.K., Ong, Y.T., Cheung, C.Y., Wong, T.Y.: Retinal Vascular Caliber Measurements: Clinical Significance, Current Knowledge and Future Perspectives. *Ophthalmologica* **229**, 125–136 (2013)
8. Li, H., Yezzi, A.: Vessels as 4-d curves: Global minimal 4-d paths to extract 3-d tubular surfaces and centerlines. *IEEE TMI* **26**, 1213–1223 (2007)
9. Mirebeau, J.-M.: Anisotropic Fast-Marching on cartesian grids using Lattice Basis Reduction. *SIAM J. Num. Anal.* **52**(4), 1573 (2014)
10. Péchaud, M., Peyré, G., Keriven, R.: Extraction of tubular structures over an orientation domain. In: *Proc. IEEE Conf. CVPR*, pp. 336–343 (2009)
11. Peyré, G., Péchaud, M., Keriven, R., Cohen, L.: Geodesic methods in computer vision and graphics. *F. Trends in Comp. Graphics and Vision* **5**(3–4), 197–397 (2010)
12. Sachkov, Y.L.: Cut locus and optimal synthesis in the sub-Riemannian problem on the group of motions of a plane. *ESAIM: COCV* **17**, 293–321 (2011)
13. Sethian, J.A.: *Level Set Methods and Fast Marching Methods*. Cambridge Univ. Press (1999)